Bioelectrochemistry 74 (2008) 90–95

Contents lists available at ScienceDirect

Bioelectrochemistry

journal homepage: www.elsevier.com/locate/bioelechem

Direct electrochemistry and electrocatalysis of horseradish peroxidase in α-zirconium phosphate nanosheet film

Xiushuang Yang, Xu Chen, Lan Yang, Wensheng Yang *

State Key Laboratory of Chemical Resource Engineering, Beijing University of Chemical Technology, Beijing 100029, China

ARTICLE INFO

Article history:
Received 30 November 2007
Received in revised form 15 April 2008
Accepted 4 May 2008
Available online 16 May 2008

Keywords:
Biosensor
Horseradish peroxidase
α-Zirconium phosphate nanosheets
Direct electrochemistry
Electrocatalysis

ABSTRACT

α-zirconium phosphate nanosheets (ZrPNS) derived via the delamination of layered α-zirconium phosphate (α-ZrP) have been proven to be efficient support matrixes for the immobilization of horseradish peroxidase (HRP). X-ray powder diffraction (XRD) results revealed that ZrPNS in HRP–ZrPNS film remained unorderly structured for the effect of HRP. Fourier transform infrared (FTIR) spectra results revealed that HRP remained the secondary structure in HRP–ZrPNS film. The direct electrochemistry of HRP was realized in HRP–ZrPNS film on a glassy carbon electrode (GCE), showing a pair of well-defined, nearly reversible cyclic voltammetry (CV) peaks for the HRP heme Fe^{III}/Fe^{II} redox couple. The average surface concentration (Γ^*) of electroactive HRP in HRP–ZrPNS film was estimated to be 1.35×10^{-10} mol cm^{-2}, which indicated a high loading of enzyme molecules in HRP–ZrPNS film. Based on these, a third generation reagentless biosensor was constructed for the determination of hydrogen peroxide (H_2O_2). The response time of the biosensor was less than 3 s, and the linear response range of the biosensor for H_2O_2 was from 1.3×10^{-6} to 1.6×10^{-2} M with a correlation coefficient of 0.9997.

1. Introduction

Direct electrochemistry of redox proteins is of immense interest both for the fundamental study of electron transfer in proteins and for the development of highly selective bioelectrocatalyst and biosensors. However, it is difficult for proteins to directly exchange electrons with the normal electrode surfaces. The electron transfer rates between the proteins and the electrode surfaces are usually prohibitively slow because of the deep burying of the electroactive prosthetic groups within the peptide chains of the proteins, the adsorptive denaturation of the proteins onto the electrode surfaces and/or the unfavorable orientation of the proteins on the electrode surfaces. Due to the difficulty of direct electron transfer between proteins and bare electrodes, some modifiers such as organic materials [1–7], inorganic materials [8–14], and inorganic/organic hybrid materials [15] have been used to promote the direct electron transfer of proteins at electrode surfaces. Because of their regular structures, good mechanical, chemical and thermal stabilities, inorganic materials are more attractive for this purpose [10–14].

Among various inorganic materials used for protein binding, the inorganic layered solids, such as metal oxides [11], clay [16] and phosphates [17–20] have attracted considerable attention. Although many kinds of biomolecules have been immobilized using layered materials as carriers, few works have been reported to investigate the direct electron transfer between the proteins immobilized in layered materials and electrodes [21–23].

Layered α-zirconium phosphate ($Zr(HPO_4)_2{\cdot}H_2O$, abbreviated as α-ZrP) is a well-characterized layered material with hydrophilic surface, thermal stability and chemical inertness, which provide a suitable medium to immobilize proteins [20]. Its structure arises by the packing of layers that consist of zirconium atoms lying in a plane and sandwiched by O_3P–OH groups situated alternatively above and below the plane [17], which can provide a biocompatible environment to the immobilized biomolecules. Lately α-ZrP was modified on the glassy carbon electrode (GCE) to promote the direct electron transfer of hemoglobin. But the inefficient electron transfer of hemoglobin was observed in the α-ZrP nanoparticle film, probably due to the weak conductivity and low enzyme-loading ability of α-ZrP nanoparticles [24].

Recently, a new class of nanomaterials — nanosheets have been synthesized via delamination of layered compounds. These lamellar crystallites exhibit colloidal and polyelectrolytic nature as well as new or enhanced physicochemical properties [25–27]. In addition, large surface areas can be obtained from nanosheets. The features above provide a potential application of nanosheets in the promotion of direct electron transfer between proteins and electrodes [14,28].

In this paper, α-ZrP nanosheets (ZrPNS) were synthesized via delamination of layered α-ZrP and used to immobilize horseradish peroxidase (HRP). Direct electrochemistry of HRP immobilized in the ZrPNS film was investigated. A pair of well-defined and nearly symmetrical redox peaks were achieved which suggested that the enhanced reversible electron transfer between HRP and GCE. The HRP

* Corresponding author. Tel.: +86 10 6443 5271; fax: +86 10 6442 5385.
E-mail address: yangws@mail.buct.edu.cn (W. Yang).

1567-5394/$ – see front matter © 2008 Elsevier B.V. All rights reserved.
doi:10.1016/j.bioelechem.2008.05.002

immobilized in ZrPNS film retained its native structure as characterized by Fourier transform infrared (FTIR) spectra. Subsequently, the direct electrochemical behavior of HRP immobilized on GCE by using thin film of ZrPNS and its electrocatalytic property for reduction of H_2O_2 were studied. We hope this HRP–ZrPNS film can find potential application in the preparation of third generation biosensors or bioreactors.

2. Experimental

2.1. Reagents

Horseradish peroxidase (HRP, EC1.11.1.7, 250 U mg^{-1}) was purchased from Dongfeng Shanghai Biochemical Technology Ltd., and polyvinyl butyral (PVB) was purchased from Sigma. H_2O_2 (30% w/w) was obtained from Beijing Chemical Plant, and its dilute solution was prepared daily. Phosphate buffer solutions (PBS, 0.10 M) with various pH were prepared by mixing standard stock solutions of Na_2HPO_4 and NaH_2PO_4. All other chemical reagents were of analytical grade and used without further purification. Water was doubly distilled in quartz apparatus, and the conductivity of the water is less than 10^{-6} S cm^{-1}.

2.2. Apparatus

Electrochemical measurements were performed with a conventional three-electrode system with the enzyme electrode as the working electrode, a platinum wire as the auxiliary electrode and an Ag/AgCl (3 M KCl) electrode as the reference electrode, against which all potentials were quoted. The electrodes were connected to a CHI 660B electrochemical workstation (ChenHua Instruments, Shanghai, China). A 10-mL electrochemical cell and a magnetic stirring bar were used. The PBS was in thoroughly anaerobic conditions by bubbling with high-purity nitrogen at least 20 min. Nitrogen environment was kept in the cell by continuously bubbling N_2 during the whole experiment. All experiments were conducted under ambient conditions at approximately 25 °C.

X-ray powder diffraction (XRD) patterns were recorded on a Shimadzu XRD-6000 X-ray diffractometer (Japan) with Cu K_α radiation at 40 kV and 30 mA. Field emission scanning electron microscope (FESEM) images were taken from a Hitachi S4700 SEM (Japan). Fourier transform infrared (FTIR) spectra were carried out on a Bruker Vector22 Fourier transform infrared spectrometer (Germany). The atomic force microscope (AFM) image of ZrPNS was achieved using a NT-MDT Model-STM Solver P47 AFM (Russia) in contact mode.

2.3. Preparation of ZrPNS colloid

The preparation of layered α-ZrP is as following. An aqueous solution A containing zirconium oxychloride and HCl and an aqueous solution B containing phosphoric acid and HCl were added simultaneously to a colloid mill rotating at 3000 rpm and mixed for 1 min. The slurry was subjected to hydrothermal treatment at 240 °C for 48 h. The resulting material was cooled to room temperature and then washed with water until pH≥6, and dried at 50 °C. The resulting material is designated as α-ZrP. 0.2 g of α-ZrP was suspended in deionized water, followed by adding 1.2 mL of 25% of tetramethylammonium hydroxide. The mixture was stirred at room temperature for 7 h with stirring bar. The suspension was then centrifuged at 10000 rpm for 5 min, and a ZrPNS colloid was obtained.

2.4. Electrode preparation

Before each experiment, glassy carbon electrodes (GCE, 3 mm diameter) were polished sequentially with 1, 0.3, and 0.05 μm α-alumina powder, with a thorough rinsing with doubly distilled water between each polishing step. The polished GCE was successively sonicated in 1:1 nitric acid, acetone and doubly distilled water, and finally allowed to dry at room temperature. The effective electrode area was obtained according to the Randles–Sevcik equation with the redox probe of $Fe(CN)_6^{3-/4-}$ [29].

To prepare the enzyme electrode, 0.1 mg of HRP was dissolved in 60 μL of the ZrPNS colloid. A polished GCE was deposited with 10 μL of the resulting mixture, and then left overnight in a refrigerator at 4 °C, and the modified electrode was abbreviated as HRP–ZrPNS/GCE. For the purpose of comparison, 10 μL of ZrPNS colloid was deposited on a polished GCE, and abbreviated as ZrPNS/GCE. After drying, they were all dipped into PVB (2% (w/v) of ethanol solution) for 1 min to enhance the adhesive ability and the stability of the films.

The enzyme electrode was stored in a refrigerator at 4 °C and rinsed with PBS prior to use.

3. Results and discussion

3.1. FESEM image of the precursor α-ZrP and AFM image of ZrPNS

To get the AFM image of ZrPNS, the samples were prepared as below: Si wafers were cleaned according to the literature [30], then the Si wafers were precoated with polyethyle nimine (PEI) by immersion in an aqueous solution of PEI (2.5 g dm^{-3}, pH=9) for 20 min to get positively charged substrates. The PEI-primed substrates were then immersed in a colloidal suspension (0.2 g dm^{-3}, pH=7) of ZrPNS for 20 min followed by thorough washing with twice-distilled water. The resulting films were dried with N_2 gas flow. The FESEM image of Fig. 1A reveals that the precursors α-ZrP are with the lateral dimensions about 500 nm and the thicknesses are about 50–80 nm (right corner of Fig. 1A). Fig. 1B shows a topographic image of the deposited layer of ZrPNS on Si wafer and the thickness of ZrPNS can be measured from the height plot in Fig. 1B. The lateral dimensions of ZrPNS obtained by AFM observation are about 400 nm and the thicknesses are about 6–8 nm.

3.2. XRD analysis of the precursor α-ZrP, ZrPNS colloid (wet state), reassembled ZrPNS, and HRP–ZrPNS film

The XRD pattern of ZrPNS colloid (wet state) was gained as follows: the ZrPNS colloid was deposited onto an XRD sample holder and measured at a constant relative humidity of 95%. The XRD patterns of reassembled ZrPNS and HRP–ZrPNS were obtained from dried ZrPNS colloid and dried HRP–ZrPNS colloid, respectively. Fig. 2A shows the XRD patterns of the precursor α-ZrP and ZrPNS colloid (wet state). The reflections in the XRD pattern of α-ZrP (Fig. 2Aa) correspond to those expected for a pure monoclinic phase of layered α-ZrP, and the position of the 002 peak corresponds to basal spacing of about 0.766 nm. The information from this XRD pattern indicates that pure phase layered α-ZrP has been obtained. As shown in Fig. 2Ab, the peaks disappear in the pattern of ZrPNS colloid (wet state), proving that α-ZrP has been successfully delaminated. Fig. 2B shows the XRD patterns of the reassembled ZrPNS and HRP–ZrPNS film. From Fig. 2Bc, we can see a reflection of the 002 peak corresponding to a basal spacing of about 0.99 nm, which is the basal spacing of TMA intercalated α-ZrP. The result shows that ZrPNS will reassemble with TMA after ZrPNS colloid being dried. As can be seen in Fig. 2Bd, the XRD pattern of dried HRP–ZrPNS film does not have any peaks. Furthermore, the XRD pattern of HRP–ZrPNS film shows no peaks at the position of lowest angle (<3°). The reason is that the added larger HRP molecules prevent ZrPNS from reassembling with TMA or HRP and make ZrPNS remain unorderly structure.

3.3. FTIR analysis of HRP and HRP–ZrPNS hybrid film

As shown in Fig. 3, the positions of amide I and II bands (1650 and 1538 cm^{-1}) of HRP (Fig. 3a) and those of HRP in the HRP–ZrPNS film

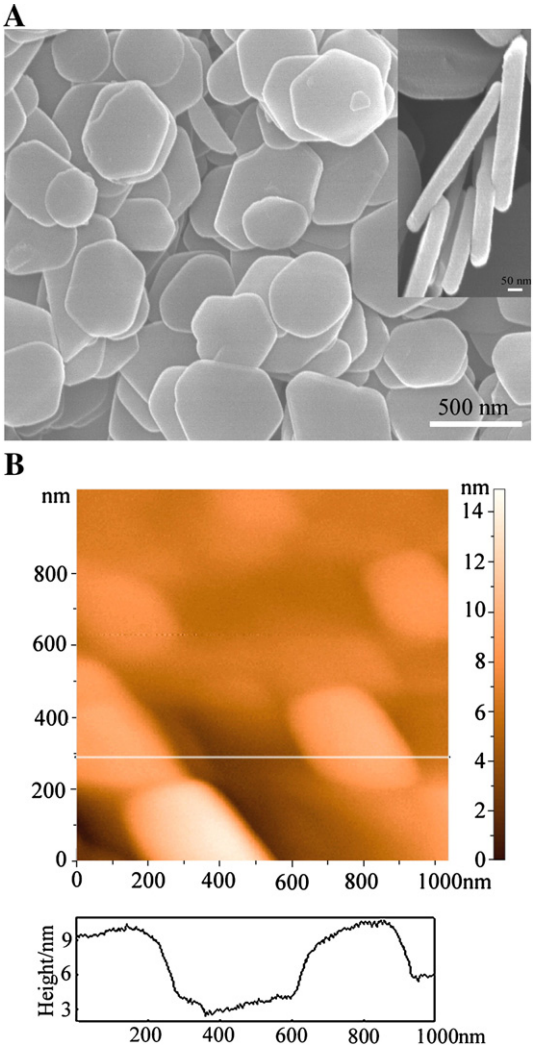

Fig. 1. FESEM image of precursor α-ZrP (A) and AFM image with height profile along the white line of ZrPNS deposited on PEI precoated Si wafer (B).

(Fig. 3b) are nearly at the same place. However, the absorption intensity of the amide I band of HRP–ZrPNS is stronger. It is enhanced by the stretching vibration of H_2O in the crystal lattice of α-ZrP at 1620 cm^{-1}, which can be seen in Fig. 3c. The strong adsorption bands at 960–1200 cm^{-1} which correspond to the flexible vibrations of P–O in the layers of α-ZrP are shown in Fig. 3b and c. The results of FTIR suggest that HRP retains the native structure in the hybrid film.

3.4. Cyclic voltammetric behavior of HRP–ZrPNS/GCE

Fig. 4 shows the cyclic voltammograms (CVs) of bare GCE, ZrPNS and HRP–ZrPNS films covered GCE in pH 7.0 PBS. There are no redox peaks for bare GCE or ZrPNS film covered GCE within the potential window of −0.7–0 V (vs. Ag/AgCl) (in Fig. 4a and b), showing that ZrPNS are not electroactive in the potential range. A well-defined, nearly reversible redox couple with the apparent formal peak potential (E^0) of −0.335 V (vs. Ag/AgCl) is observed for the HRP–ZrPNS film covered GCE (Fig. 4c), which is the characteristic of the HRP heme Fe^{III}/Fe^{II} redox couple. The value of E^0 for HRP in this work is very close to those reported for immobilized HRP entrapped in various films [5,6,11]. The peak-to-peak separation (ΔE_p) is 35 mV (vs. Ag/AgCl) at a scan rate of 50 mV s^{-1}, indicating the nearly reversible direct electron transfer of HRP heme Fe^{III}/Fe^{II}. Both the cathodic peak current (i_{pc}) and the anodic peak current (i_{pa}) increase linearly with the scan rate up to 300 mV s^{-1} (Fig. 5), which is the characteristic of thin-layer electrochemistry. The

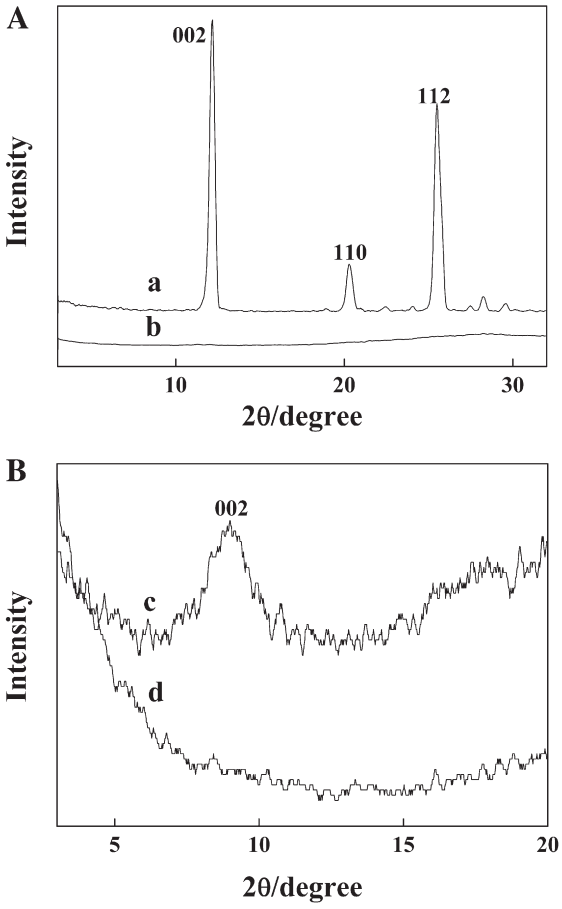

Fig. 2. A. XRD patterns of (a) precursor α-ZrP, and (b) ZrPNS colloid (wet state), B. XRD patterns of (c) reassembled ZrPNS, and (d) HRP–ZrPNS film.

ratios of i_{pc} to i_{pa} are within 0.98–1.02, indicating that there are no kinetic or other complications in the electrode process, that is, almost all electroactive met-HRP in the membrane are converted to oxy-HRP on the forward cyclic voltammetry (CV) sweep and vice versa. By integration of the anodic peaks in CVs, the charges, and the effective electrode area, thus the average surface concentration (Γ^*) of electroactive species can be calculated. The Γ^* of electroactive HRP in ZrPNS film is estimated to be 1.35×10^{-10} mol cm^{-2}, which is almost seven times than that of the theoretical monolayer coverage (about 2×10^{-11} mol cm^{-2}). This indicates that multilayers of HRP in the HRP–

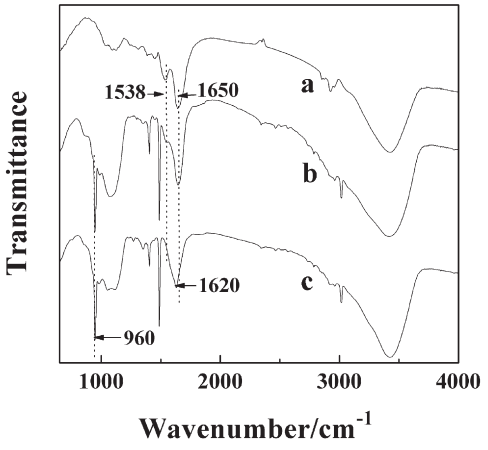

Fig. 3. FTIR spectra of (a) HRP, (b) HRP–ZrPNS, and (c) ZrPNS.

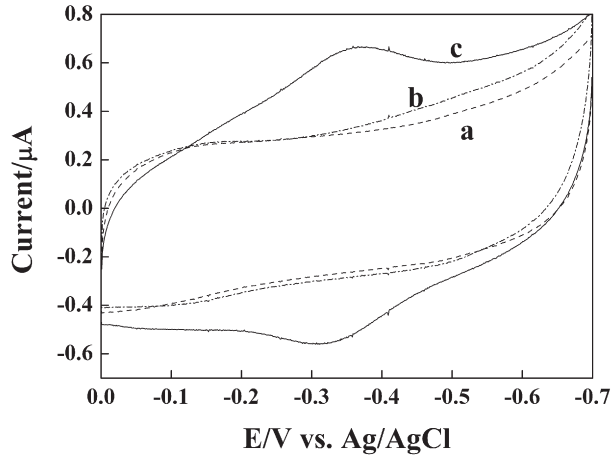

Fig. 4. Cyclic voltammograms of (a) bare GCE, (b) ZrPNS/GCE, and (c) HRP–ZrPNS/GCE in 0.1 M PBS (pH 7.0), scan rate: 50 mV s^{-1}.

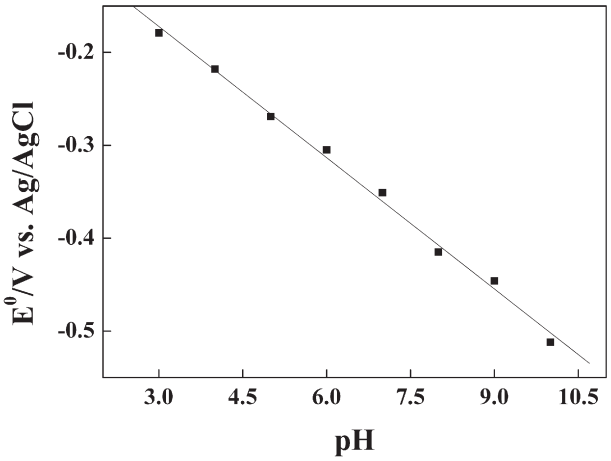

Fig. 6. Effect of pH on formal potential (E^0) of HRP–ZrPNS/GCE in 0.1 M PBS.

ZrPNS film have participated in the electron transportation process. Because the multilayers of HRP were far from the electrode surface, it was impossible for them to exchange electrons directly with the electrode [31]. Thus, the electron transportation process most likely occurred as charge-hopping, which was similar to the heme-containing LBL films previously reported [32]. The value of Γ^* obtained in this paper is larger than $(9.10\pm0.15)\times10^{-11}$ mol cm^{-2} of HRP in Eastman AQ films [5], 2.62×10^{-11} mol cm^{-2} of HRP in agarose hydrogel films in room-temperature ionic liquids [7], and 8.5×10^{-11} mol cm^{-2} obtained at HRP intercalated into layered titanate nanosheets modified GCE [14], indicating a high loading of enzyme molecules in ZrPNS films, which comes from large surface area and many negative charges of ZrPNS.

The electron transfer rate (k_s) of HRP ($n=1$) in the hybrid film was evaluated based on the equation derived by Laviron [33] for diffusionless CV with $n\Delta E_p<200$ mV:

$$k_s = mnFv/RT \quad (1)$$

Where m is a parameter related to ΔE_p. According to the ΔE_p of the CVs of the HRP–ZrPNS film covered GCE at the scan rate of 300 mV s^{-1}, the k_s value of HRP in this work is 7.8 s^{-1}.

The influence of pH on the voltammetry of HRP–ZrPNS film was examined (Fig. 6). An increase of pH of PBS from 3.0 to 10.0 causes a negative shift in both anodic and cathodic peak potentials of HRP–ZrPNS film, indicating that hydrogen ion is involved in the electrode reaction of HRP. In addition, all changes in voltammetric peak potentials and currents with pH are reversible. That is, the same CV curve is reproduced after immersion in a solution with a different pH and then return to its original solution. The slope of the E^0 versus pH plot is 47.08 mV pH^{-1}. The value is smaller than the theoretically expected value of 59 mV pH^{-1} for the transfer of one proton and one electron per heme group during the electrode reaction. The same results were obtained for HRP-gelatin-OMIM·PF_6/GCE [34] and HRP–PNM/GCE [35]. The clear explanation for this was not yet known. According to the literature [34,35], it might be that the influence of the protonation states of trans ligands to the heme iron and amino acids around the heme, or the protonation of the water molecule coordinated to the central iron.

The stability of HRP–ZrPNS film was investigated. The electrode can keep a constant current during sweeping 100 cycles in the blank PBS. The peak currents decrease about 12% after the electrodes have been stored in refrigerator at 4 °C for 2 months.

3.5. Electrocatalytic behavior of HRP–ZrPNS/GCE

Electrocatalytic reduction of H_2O_2 was examined by measuring CVs using the HRP–ZrPNS film modified GCE. Fig. 7 shows CVs of HRP–ZrPNS film modified GCE and ZrPNS covered GCE in the absence or the presence of H_2O_2. The cathodic peak (−0.32 V vs. Ag/AgCl) of HRP–ZrPNS film modified GCE is greatly enhanced in the presence of H_2O_2, while the corresponding anodic peak decreases, suggesting that an electrocatalytic reduction of H_2O_2 occurred. The i_{pc} value increases

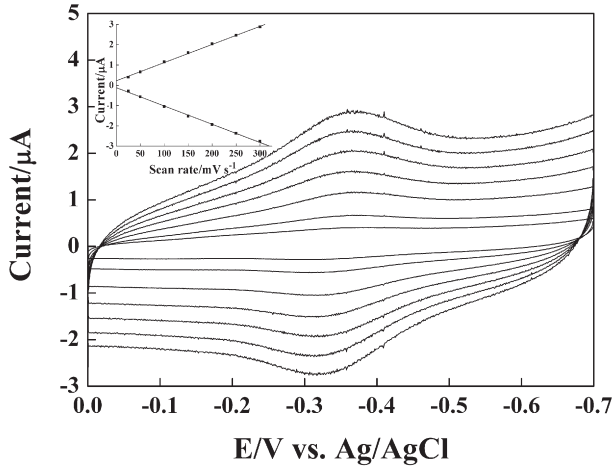

Fig. 5. Cyclic voltammograms of HRP–ZrPNS/GCE in 0.1 M PBS (pH 7.0) at different scan rates (from inner to outer): 25, 50, 100, 150, 200, 250, 300 mV s^{-1}. Plots of cathodic and anodic peak currents vs. scan rates are in the left corner.

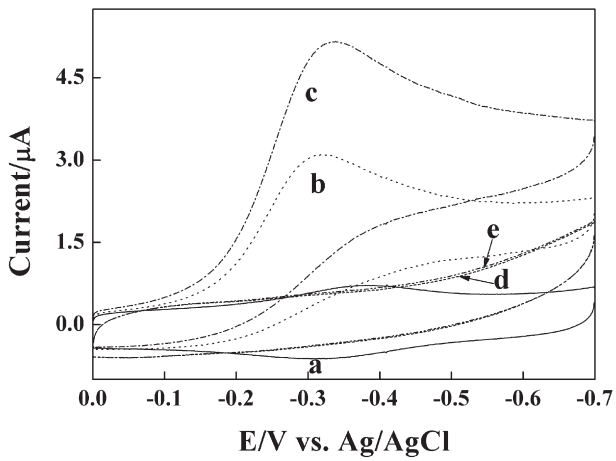

Fig. 7. Cyclic voltammograms of HRP–ZrPNS/GCE in the absence (a) and presence of 0.1 mM (b), and 0.2 mM (c) H_2O_2, and ZrPNS/GCE in the absence (d) and presence of 0.2 mM (e) H_2O_2 at a scan rate of 50 mV s^{-1} in 0.1 M PBS (pH 7.0).

with increasing the concentration of H_2O_2. The same phenomenon is observed in other references [5,6,11,14]. No peaks are observed at the ZrPNS covered GCE in the presence of H_2O_2.

The pH dependence of the enzyme electrode was investigated over the pH range 3.0–10.0 in 0.1 M PBS in the presence of 0.1 mM H_2O_2. The optimum biosensor response is achieved at pH 7.0. Lowering or increasing the pH result in a decrease of biocatalyst activity. This result is close to those reported for immobilized HRP entrapped in various films [5,6,11,14,15]. This indicates that the optimum pH value of HRP is not affected by the film components. Therefore, pH 7.0 has been selected for the subsequent studies since the maximum response is obtained at this pH.

To further investigate the bioactivity of immobilized HRP, we used this biosensor to determine H_2O_2. Fig. 8 shows the calibration curve, and the inset picture of Fig. 8 shows the response curve for the biosensor at optimized conditions on successive injection of 0.01 mM H_2O_2 to stirring PBS at pH 7.0. The biosensor achieves 95% of the steady-state current within 3 s. It is more rapid than those of many other modified electrodes [15]. The linear range of the biosensor is 1.3×10^{-6}–1.6×10^{-2} M H_2O_2, with a correlation coefficient of 0.9997 ($n=16$). The detection limit of the biosensor is 1.2 μM H_2O_2 based on $S/N=3$. The linear range of the enzyme electrode is wider than those of many enzyme electrodes [6,11,14,15,36,37]. The wide linear range of the enzyme electrode in our work may come from the good biocompatibility of ZrPNS, which makes the immobilized HRP maintain high biocatalyst activity in a wide range of H_2O_2 concentration.

The reproducibility of the response of the enzyme electrode was investigated at a 0.1 mM H_2O_2 concentration. The relative standard deviation determined by six analyses of a 0.1 mM H_2O_2 standard using a single enzyme electrode was found to be about 7.0%. For five enzyme electrodes made from the same batch, a relative standard deviation of about 3.0% was obtained for the individual current response for the same sample (0.1 mM H_2O_2).

The stability of the biosensor under storage was investigated by measuring the biosensor response with 0.1 mM of H_2O_2 every 4 days over 2 months period. Up to 16 days, the current response remains 99% of the initial value. When the modified electrode has been stored in dry for 60 days at 4 °C, the electrode retains about 85% of its initial response current to 0.1 mM H_2O_2, indicating that the enzyme electrode has a good stability. The long-term stability of the HRP–ZrPNS modified GCE can be attributed to two reasons. One is that the large number of hydroxyl groups of ZrPNS will provide an aqueous-like microenvironment to stabilize the immobilized proteins. The other is that the ZrPNS has the negative charge, which is contrary to the HRP when pH value is 7.0 (HRP, pI=8.9). The opposite charge can improve the immobilization of enzyme and prevent the leakage of enzyme [38,39], so the life-span of the biosensor is increased. The good storage stability suggests that the ZrPNS are suitable matrixes for immobilization of HRP to retain its activity and prevent it from leaking out from the film.

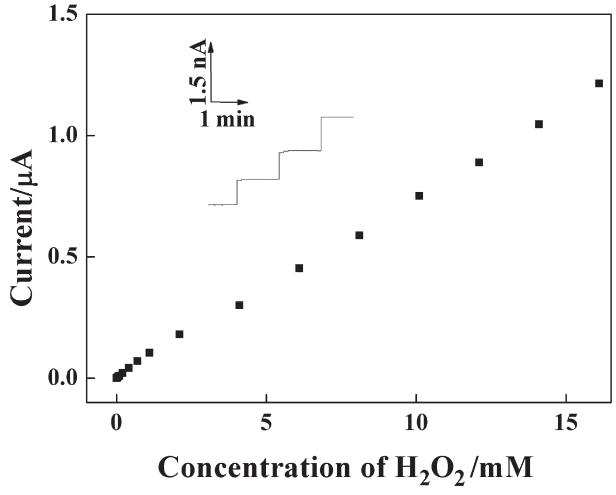

Fig. 8. Calibration curve of the enzyme electrode. The inset figure shows some ladders from the dynamic response of the enzyme electrode to successive addition of 0.01 mM H_2O_2 to 0.1 M PBS (pH 7.0). The applied potential is −0.25 V vs. Ag/AgCl.

4. Conclusion

ZrPNS was prepared by the delamination of layered α-ZrP and used to immobilize HRP. The results of FTIR indicate that HRP incorporated in ZrPNS film basically retains its native secondary structure. A well-defined, quasi-reversible, stable redox couple has been obtained for HRP in HRP–ZrPNS film. The entrapped HRP exhibits good electroactivity, bioactivity, and electrocatalytic activity due to the specialities of ZrPNS, such as the hydrophilic surface, large surface area, and so on. The HRP–ZrPNS films are stabilized by hydrophilic and Coulombic interactions between HRP and ZrPNS. The results suggest that ZrPNS are suitable matrixes for the immobilization of enzymes to retain their activities. The HRP–ZrPNS modified GCE may have potential use in the fabrication of third generation biosensors and bioreactors.

Acknowledgments

We gratefully acknowledge the financial support from the National 863 Project (Grant No. 2006AA03Z343), the National Natural Science Foundation of China, the 111 Project (Grant No. B07004), and Program for Changjiang Scholars and Innovative Research Team in University (Grant No. IRT0406).

References

[1] L. Shen, N. Hu, Electrostatic adsorption of heme proteins alternated with polyamidoamine dendrimers for layer-by-layer assembly of electroactive films, Biomacromole. 6 (2005) 1475–1483.
[2] X. Lu, J. Hu, X. Yao, Z. Wang, J. Li, Composite system based on chitosan and room-temperature ionic liquid: direct electrochemistry and electrocatalysis of hemoglobin, Biomacromole. 7 (2006) 975–980.
[3] X. Liu, Y. Xu, X. Ma, G. Li, A third-generation hydrogen peroxide biosensor fabricated with hemoglobin and Triton X-100, Sens. Actu. B 106 (2005) 284–288.
[4] F. Yin, H.K. Shin, Y.S. Kwon, A hydrogen peroxide biosensor based on Langmuir–Blodgett technique: direct electron transfer of hemoglobin in octadecylamine layer, Talanta 67 (2005) 221–226.
[5] R. Huang, N. Hu, Direct electrochemistry and electrocatalysis with horseradish peroxidase in Eastman AQ films, Bioelectrochem. 54 (2001) 75–81.
[6] Y. Wu, Q. Shen, S. Hu, Direct electrochemistry and electrocatalysis of heme-proteins in regenerated silk fibroin film, Anal. Chim. Acta 558 (2006) 179–186.
[7] S.F. Wang, T. Chen, Z.L. Zhang, X.C. Shen, Z.X. Lu, D.W. Pang, K.Y. Wong, Direct electrochemistry and electrocatalysis of heme proteins entrapped in agarose hydrogel films in room-temperature ionic liquids, Langmuir 21 (2005) 9260–9266.
[8] G.C. Zhao, Z.Z. Yin, L. Zhang, X.W. Wei, Direct electrochemistry of cytochrome c on a multi-walled carbon nanotubes modified electrode and its electrocatalytic activity for the reduction of H_2O_2, Electrochem. Commun. 7 (2005) 256–260.
[9] J. Wang, M. Li, Z. Shi, N. Li, Z. Gu, Direct electrochemistry of cytochrome c at a glassy carbon electrode modified with single-wall carbon nanotubes, Anal. Chem. 74 (2002) 1993–1997.
[10] H. Zhang, H. Lu, N. Hu, Fabrication of electroactive layer-by-layer films of myoglobin with gold nanoparticles of different sizes, J. Phys. Chem. B 110 (2006) 2171–2179.
[11] Y. Zhang, P. He, N. Hu, Horseradish peroxidase immobilized in TiO_2 nanoparticle films on pyrolytic graphite electrodes: direct electrochemistry and bioelectrocatalysis, Electrochim. Acta 49 (2004) 1981–1988.
[12] A. Liu, M. Wei, I. Honma, H. Zhou, Direct electrochemistry of myoglobin in titanate nanotubes film, Anal. Chem. 77 (2005) 8068–8074.
[13] Q. Wang, G. Lu, B. Yang, Direct electrochemistry and electrocatalysis of hemoglobin immobilized on carbon paste electrode by silica sol–gel film, Biosens. Bioelectron. 19 (2004) 1269–1275.
[14] L. Zhang, Q. Zhang, X. Lu, J. Li, Direct electrochemistry and electrocatalysis based on film of horseradish peroxidase intercalated into layered titanate nano-sheets, Biosens. Bioelectron. 23 (2007) 102–106.
[15] Y. Xiao, H.X. Ju, H.Y. Chen, Direct electrochemistry of horseradish peroxidase immobilized on a colloid/cysteamine-modified gold electrode, Anal. Biochem. 278 (2000) 22–28.
[16] K.A. Carrado, S.M. Macha, D.M. Tiede, Effects of surface functionalization and organo-tailoring of synthetic layer silicates on the immobilization of cytochrome c, Chem. Mater. 16 (2004) 2559–2566.

[17] F. Bellezza, A. Cipiciani, U. Costantino, M.E. Negozio, Zirconium phosphate and modified zirconium phosphates as supports of lipase. preparation of the composites and activity of the supported enzyme, Langmuir 18 (2002) 8737–8742.
[18] C.V. Kumar, A. Chaudhari, Unusual thermal stabilities of some proteins and enzymes bound in the galleries of layered a-Zr(IV)phosphate/phosphonates, Micropor. Mesopor. Mater. 57 (2003) 181–190.
[19] A. Chaudhari, J. Thota, C.V. Kumar, Binding and cleavage studies of two proteins intercalated at the galleries of α-zirconium phosphate, Micropor. Mesopor. Mater. 75 (2004) 281–291.
[20] C.V. Kumar, A. Chaudhari, Proteins immobilized at the galleries of layered α-zirconium phosphate: structure and activity studies, J. Am. Chem. Soc. 122 (2000) 830–837.
[21] V.V. Shumyantseva, Y.D. Ivanov, N. Bistolas, F.W. Scheller, A.I. Archakov, U. Wollenberger, Direct electron transfer of cytochrome P450 2B4 at electrodes modified with nonionic detergent and colloidal clay nanoparticles, Anal. Chem. 76 (2004) 6046–6052.
[22] Y. Zhou, N. Hu, Y. Zeng, J.F. Rusling, Heme protein–clay films: direct electrochemistry and electrochemical catalysis, Langmuir 18 (2002) 211–219.
[23] Y. Zhou, Z. Li, N. Hu, Y. Zeng, J.F. Rusling, Layer-by-layer assembly of ultrathin films of hemoglobin and clay nanoparticles with electrochemical and catalytic activity, Langmuir 18 (2002) 8573–8579.
[24] J.J. Feng, J.J. Xu, H.Y. Chen, Synergistic effect of zirconium phosphate and Au nanoparticles on direct electron transfer of hemoglobin on glassy carbon electrode, J. Electroanal. Chem. 585 (2005) 44–50.
[25] F. Carn, A. Derré, W. Neri, O. Babot, H. Deleuze, R. Backov, Shaping zirconium phosphate α-$Zr(HPO_4)_2{\cdot}H_2O$: from exfoliation to first α-ZrP 3D open-cell macrocellular foams, New J. Chem., 29 (2005) 1346–1350.
[26] Y. Omomo, T. Sasaki, L. Wang, M. Watanabe, Redoxable nanosheet crystallites of MnO_2 derived via delamination of a layered manganese oxide, J. Am. Chem. Soc. 125 (2003) 3568–3575.
[27] T. Sasaki, M. Watanabe, H. Hashizume, H. Yamada, H. Nakazawa, Macromolecule-like aspects for a colloidal suspension of an exfoliated titanate. Pairwise association of nanosheets and dynamic reassembling process initiated from it, J. Am. Chem. Soc. 118 (1996) 8329–8335.
[28] H. Xiao, X. Chen, L. Ji, X. Zhang, W. Yang, Direct electrochemistry of myoglobin in MnO_2 nanosheet film, Chem. Lett. 36 (2007) 772–773.
[29] M.P. Siswana, K.I. Ozoemena1, T. Nyokong, Electrocatalysis of asulam on cobalt phthalocyanine modified multi-walled carbon nanotubes immobilized on a basal plane pyrolytic graphite electrode, Electrochim. Acta 52 (2006) 114–122.
[30] L. Wang, Y. Omomo, N. Sakai, K. Fukuda, I. Nakai, Y. Ebina, K. Takada, M. Watanabe, T. Sasaki, Fabrication and characterization of multilayer ultrathin films of exfoliated MnO_2 nanosheets and polycations, Chem. Mater. 15 (2003) 2873–2878.
[31] L. Zhang, Q. Zhang, J. Li, Layered Titanate nanosheets intercalated with myoglobin for direct electrochemistry, Adv. Funct. Mater. 17 (2007) 1958–1965.
[32] M. Majda, in: R.W. Murray (Ed.), Molecular Design of Electrode Surfaces, Wiley, New York, 1992, p. 159.
[33] E. Laviron, General expression of the linear potential sweep voltammogram in the case of diffusionless electrochemical systems, J. Electroanal. Chem. 101 (1979) 19–28.
[34] Y.X. Suna, J.T. Zhang, S.W. Huang, S.F. Wang, Hydrogen peroxide biosensor based on the bioelectrocatalysis of horseradish peroxidase incorporated in a new hydrogel film, Sens. Actuators, B 124 (2007) 494–500.
[35] R. Yan, F. Zhao, J. Li, F. Xiao, S. Fan, B. Zeng, Direct electrochemistry of horseradish peroxidase in gelatin-hydrophobic ionic liquid gel films, Electrochim. Acta 52 (2007) 7425–7431.
[36] V.S. Tripathi, V.B. Kandimalla, H. Ju, Amperometric biosensor for hydrogen peroxide based on ferrocene-bovine serum albumin and multiwall carbon nanotube modified ormosil composite, Biosens. Bioelectron. 21 (2006) 1529–1535.
[37] J. Di, C. Shen, S. Peng, Y. Tu, S. Li, A one-step method to construct a third-generation biosensor based on horseradish peroxidase and gold nanoparticles embedded in silica sol–gel network on gold modified electrode, Anal. Chim. Acta 553 (2005) 196–200.
[38] X. Chen, G. Cheng, S. Dong, Amperometric tyrosinase biosensor based on a sol–gel-derived titanium oxide–copolymer composite matrix for detection of phenolic compounds, Analyst 126 (2001) 1728–1732.
[39] Z. Liu, B. Liu, J. Kong, J. Deng, Probing trace phenols based on mediator-free alumina sol–gel-derived tyrosinase biosensor, Anal. Chem. 72 (2000) 4707–4712.